

Natural convection of nanofluid over vertical plate embedded in porous medium: prescribed surface heat flux*

A. NOGHREHABADI, A. BEHSERESHT, M. GHALAMBAZ

(Department of Mechanical Engineering, Shahid Chamran University
 of Ahvaz, Ahvaz 6135743337, Iran)

Abstract The aim of the present paper is to analyze the natural convection heat and mass transfer of nanofluids over a vertical plate embedded in a saturated Darcy porous medium subjected to surface heat and nanoparticle fluxes. To carry out the numerical solution, two steps are performed. The governing partial differential equations are firstly simplified into a set of highly coupled nonlinear ordinary differential equations by appropriate similarity variables, and then numerically solved by the finite difference method. The obtained similarity solution depends on four non-dimensional parameters, i.e., the Brownian motion parameter (N_b), the Buoyancy ratio (N_r), the thermophoresis parameter (N_t), and the Lewis number (Le). The variations of the reduced Nusselt number and the reduced Sherwood number with N_b and N_t for various values of Le and N_r are discussed in detail. Simulation results depict that the increase in N_b , N_t , or N_r decreases the reduced Nusselt number. An increase in the Lewis number increases both of the reduced Nusselt number and the Sherwood number. The results also reveal that the nanoparticle concentration boundary layer thickness is much thinner than those of the thermal and hydrodynamic boundary layers.

Key words natural convection, porous medium, nanofluid, surface heat flux, surface nanoparticle flux

Chinese Library Classification O351.2, O414.1

2010 Mathematics Subject Classification 74F10, 76N20, 76A05

Nomenclature

C ,	constant from the integration of Eq. (23);	N_b ,	Brownian motion parameter;
D_B ,	Brownian diffusion coefficient;	N_r ,	buoyancy ratio;
D_T ,	thermophoretic diffusion coefficient;	N_t ,	thermophoresis parameter;
f ,	rescaled nanoparticle volume fraction,	p ,	pressure;
	nanoparticle concentration;	q_{np} ,	nanoparticle flux;
g ,	gravitational acceleration vector;	q_w ,	wall heat flux of the vertical plate;
K ,	permeability of the porous medium;	Ra_x ,	local Rayleigh number;
k ,	thermal conductivity;	S ,	dimensionless stream function;
k_m ,	effective thermal conductivity;	T ,	temperature;
Le ,	Lewis number;	T_∞ ,	ambient temperature;

* Received Apr. 12, 2012 / Revised Jan. 13, 2013

Corresponding author A. NOGHREHABADI, Ph.D., E-mail: a.r.noghrehabadi@scu.ac.ir

T_w ,	wall temperature of the vertical plate;	u, v ,	Darcy velocity components;
U ,	reference velocity;	x, y ,	Cartesian coordinates.

Greek symbols

$(\rho c)_f$,	heat capacity of the fluid;	λ ,	index in the power-law variation of the wall heat and mass flux;
$(\rho c)_p$,	effective heat capacity of the nanoparticle material;	ρ_f ,	fluid density;
μ ,	viscosity of the fluid;	ρ_p ,	nanoparticle mass density;
α_m ,	effective thermal diffusivity defined by Eq. (5);	τ ,	parameter defined by Eq. (5);
β ,	volumetric expansion coefficient of the fluid;	ϕ ,	nanoparticle volume fraction;
ε ,	porosity;	ϕ_∞ ,	ambient nanoparticle volume fraction;
η ,	dimensionless distance defined by Eq. (5);	ϕ_w ,	nanoparticle volume fraction at the wall of the vertical plate;
θ ,	dimensionless temperature;	ψ ,	stream function.

1 Introduction

The analysis and simulation of natural convection in saturated porous media have many important engineering and geophysical applications, e.g., flow through filtering media, thermal energy storage, groundwater systems for industrial usage, and crude oil extraction^[1]. The prediction of the natural convection heat transfer characteristics from heated bodies embedded in a porous medium is crucial to the design of canisters for nuclear waste disposal. A similarity solution for natural convection along a vertical plate in a porous medium was presented by Cheng and Minkowycz^[2]. In their work^[2], the wall temperature of the surface was assumed to be a function of the distance from the origin. The Nusselt number was found to increase with the increase in the power index of the wall temperature. With the scale analysis method, Bejan and Khair^[3] studied the heat and mass transfer by natural convection over a vertical plate embedded in a Darcy porous medium. They demonstrated that the natural convection conformed to different possible flow regimes, depending on the buoyancy ratio and the Lewis number. Kaviani and Mittal^[4] performed an experimental study to obtain the magnitude of the local heat transfer rate from a vertical plate embedded in a saturated porous medium.

Hassanien^[5] investigated the effects of variable surface heat flux boundary conditions and porous medium permeabilities on the mixed convection past a vertical wedge placed in a saturated porous medium. They showed that an increase in the power index of the wall heat flux would decrease the thermal boundary layer thickness and increase the temperature gradient in the boundary layer. Hsieh et al.^[6] presented a non-similarity solution for mixed convection heat transfer over vertical surfaces with variable surface temperature/heat flux.

Recently, nanotechnology has had a rapid development speed and led to generate a new class of fluids, i.e., nanofluids, with high potential in heat transfer. Nanofluids are produced by suspending nanoparticles, metallic or nonmetallic particles of nanometer dimensions, in conventional heat transfer fluids such as water, oil, and ethylene glycol. Compared with conventional microfluid suspensions, nanofluids usually do not have rapid settling down problems. Nanofluids, as new coolants, have shown enhanced thermophysical properties for heat transfer applications. Lee et al.^[7] and Wang et al.^[8] reported that dispersing 10% (volume fraction) of CuO nanoparticles (with the sizes of 23 nm and 24 nm) in the water would increase the thermal conductivity of the base fluid by 34%. Li and Peterson^[9] experimentally found that a low volume fraction (6%) of Al₂O₃ nanoparticles, dispersed in water, would increase the thermal conductivity of water up to 28.2%. Therefore, nanofluids are being used or considered for utilization in many devices to enhance the heat transfer efficiency^[10–14].

The heat transfer of nanofluids in a porous medium is a new subject. Only a few researches have been performed in this area. Ahmad and Pop^[15] analyzed a mixed convection boundary layer of nanofluid flows over a vertical plate embedded in a porous medium. Hady et al.^[16] investigated the natural convection boundary layer flow around a vertical isothermal cone embedded in a porous medium filled with a nanofluid. In both the studies of Ahmad and Pop^[15] and Hady et al.^[16], it was assumed that there was a uniform mixture of nanoparticles, and thus there was not any concentration gradient of nanoparticles in the mixture.

Recently, Nield and Kuznetsov^[17] analyzed the boundary layer flow of a nanofluid in a saturated porous media. The nanofluid model, employing the Darcy model, incorporated the concentration gradient of nanoparticles due to the effects of the Brownian motion and thermophoresis. It was reported that the Brownian motion and thermophoresis parameters significantly influenced the reduced Nusselt number. Gorla et al.^[1] studied the mixed convective boundary layer of the nanofluid flow past a vertical wedge placed in a porous medium. Gorla and Chamkha^[18] investigated the natural convection of the nanofluid flow over a horizontal plate placed in a porous medium. In the above works^[1,15–18], the case of prescribed wall temperature for the wall surface was considered. However, in practical applications, the boundary conditions sometimes are approximated by a heat flux boundary condition^[19]. In many applications, the hot surface may be subject to a constant heat flux instead of being at a constant temperature. For example, an embedded electronic component on a circuit board can be pre-defined a heat power, but the temperature of the component is not known. Moreover, the rate of heat generation in the canisters of nuclear waste disposal is known, and hence the heat flux on the surface of these containers is known.

Nield and Kuznetsov^[17] previously studied the natural convective boundary layer flow past a vertical plate embedded in a porous medium filled with a nanofluid subjected to a constant surface temperature. Following Nield and Kuznetsov^[17] and because of the wide applications of the heat flux boundary condition, the case of the constant surface heat flux boundary condition is considered in the present study. The objective of the present paper is to analyze the steady natural convection flow of a nanofluid over a vertical plate embedded in a saturated porous medium subjected to the surface heat and mass fluxes. The nanofluid model, utilized in the present study, incorporates the dynamic effects of nanoparticles, including the Brownian motion and thermophoresis. A similarity solution, depending on the buoyancy ratio parameter, the Lewis number, the Brownian motion parameter, and the thermophoresis parameter, is obtained. The effects of these four parameters on the reduced Nusselt number and the Sherwood number are numerically investigated.

2 Mathematical formulations

Consider a two-dimensional natural convection boundary layer flow past along a vertical plate placed in a porous medium saturated with a nanofluid. It is assumed that the flow is incompressible and steady-state. The plate surface is imposed to the surface heat flux and the nanoparticle flux. The coordinate system is chosen such that the x -axis is aligned with the flow on the plate. A schematic view of the physical model and coordinate system are shown in Fig.1. As shown in this figure, there are three different boundary layers, i.e., the hydrodynamic boundary layer, the thermal boundary layer, and the nanoparticle concentration boundary layer. The ambient values of the temperature and nanoparticle concentrations are denoted by T_∞ and φ_∞ , respectively, as y tends to infinity. The flow in the homogeneous porous medium with the porosity ε and the permeability K is considered as Darcy flow, and the Oberbeck-Boussinesq approximation is employed. Furthermore, the porous medium and nanofluid are assumed in the local thermal equilibrium.

With the standard boundary layer approximations, the steady-state conservation of the total mass, the momentum, the energy, and the conservation of nanoparticles for nanofluids over a

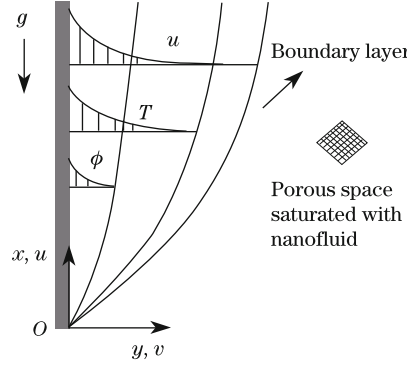


Fig. 1 Physical model and coordinate systems utilized to model convective heat transfer past vertical plate embedded inside homogeneous porous medium saturated with nanofluid

heated surface embedded in a saturated porous medium are presented as follows^[1,17]:

$$\frac{\partial u}{\partial x} + \frac{\partial v}{\partial y} = 0, \quad (1)$$

$$\begin{cases} \frac{\partial p}{\partial y} = 0, \\ \frac{\mu}{K} u = -\left(\frac{\partial p}{\partial x} - (1 - \phi_\infty) \beta g \rho_{f_\infty} (T - T_\infty)\right) - (\rho_p - \rho_{f_\infty}) g (\phi - \phi_\infty), \end{cases} \quad (2)$$

$$u \frac{\partial T}{\partial x} + v \frac{\partial T}{\partial y} = \alpha_m \nabla^2 T + \tau \left(D_B \frac{\partial \phi}{\partial y} \frac{\partial T}{\partial y} + \frac{D_T}{T_\infty} \left(\frac{\partial T}{\partial y} \right)^2 \right), \quad (3)$$

$$\frac{1}{\varepsilon} \left(u \frac{\partial \phi}{\partial x} + v \frac{\partial \phi}{\partial y} \right) = D_B \frac{\partial^2 \phi}{\partial y^2} + \frac{D_T}{T_\infty} \frac{\partial^2 T}{\partial y^2}, \quad (4)$$

where α_m and τ are defined as

$$\begin{cases} \alpha_m = \frac{k_m}{(\rho c)_f}, \\ \tau = \frac{\varepsilon (\rho c)_p}{(\rho c)_f}. \end{cases} \quad (5)$$

Based on the problem description, the boundary conditions are taken to be

$$v = 0, \quad -\frac{\partial T}{\partial y} \Big|_{y=0} = \frac{q_w}{k}, \quad -\frac{\partial \phi}{\partial y} \Big|_{y=0} = \frac{q_{np}}{D_B} \quad \text{at } y = 0, \quad x \geq 0, \quad (6)$$

$$u \rightarrow u_\infty, \quad T \rightarrow T_\infty, \quad \phi \rightarrow \phi_\infty \quad \text{at } y \rightarrow \infty, \quad (7)$$

where q_w is the surface heat flux, and q_{np} is the surface nanoparticle flux. Both of the fluxes are assumed to be proportional to x^λ , i.e.,

$$q_w'' = ax^\lambda, \quad q_{np}'' = bx^\lambda,$$

where the exponent λ is a real value.

The pressure p can be eliminated from Eq. (2) by cross-differentiation, and the continuity equation will be automatically satisfied by introducing the following stream function (ψ):

$$u = \frac{\partial \psi}{\partial y}, \quad v = -\frac{\partial \psi}{\partial x}. \quad (8)$$

Now, the governing differential equations can be reduced to the following three differential equations:

$$\frac{\partial^2 \psi}{\partial y^2} = \frac{(1 - \phi_\infty) \rho_{f\infty} \beta g K}{\mu} \frac{\partial T}{\partial y} - \frac{(\rho_p - \rho_{f\infty}) g K}{\mu} \frac{\partial \phi}{\partial y}, \quad (9)$$

$$\frac{\partial \psi}{\partial y} \frac{\partial T}{\partial x} - \frac{\partial \psi}{\partial x} \frac{\partial T}{\partial y} = \alpha_m \frac{\partial^2 T}{\partial y^2} + \tau \left(D_B \frac{\partial \phi}{\partial y} \frac{\partial T}{\partial y} + \frac{D_T}{T_\infty} \left(\frac{\partial T}{\partial y} \right)^2 \right), \quad (10)$$

$$\frac{1}{\varepsilon} \left(\frac{\partial \psi}{\partial y} \frac{\partial \phi}{\partial x} - \frac{\partial \psi}{\partial x} \frac{\partial \phi}{\partial y} \right) = D_B \frac{\partial^2 \phi}{\partial y^2} + \frac{D_T}{T_\infty} \frac{\partial^2 T}{\partial y^2}. \quad (11)$$

Here, the local Rayleigh number (Ra_x) is introduced as

$$Ra_x = \frac{(1 - \phi_\infty) \rho_{f\infty} \beta g x q_w x}{\mu \alpha_m k}. \quad (12)$$

To simplify the system of Eqs. (9)–(11) and attain a similarity solution to Eqs. (9)–(11) subjected to Eqs. (6) and (7), the similarity variable η is given by

$$\eta = \frac{y}{x} Ra_x^{\frac{1}{3}}, \quad (13)$$

and the dimensionless similarity quantities S , θ , and f are

$$\begin{cases} S = \frac{\psi}{\alpha_m Ra_x^{\frac{1}{3}}}, \\ f = \frac{(\phi - \phi_\infty) D_B}{q_{np} x} Ra_x^{\frac{1}{3}}, \\ \theta = \frac{k(T - T_\infty)}{q_w x} Ra_x^{\frac{1}{3}}. \end{cases} \quad (14)$$

The governing equations can be reduced to three coupled ordinary differential equations. Applying Eqs. (13) and (14) on Eqs. (6)–(7) and (9)–(11) yields the following ordinary differential equations:

$$S'' - \theta' + N_r f' = 0, \quad (15)$$

$$\theta'' + \frac{\lambda + 2}{3} S \theta' - \frac{2\lambda + 1}{3} S' \theta + N_b f' \theta' + N_t (\theta')^2 = 0, \quad (16)$$

$$f'' + \frac{\lambda + 2}{3} L_e S f' - \frac{2\lambda + 1}{3} L_e f S' + \frac{N_t}{N_b} \theta'' = 0 \quad (17)$$

subjected to the following boundary conditions (see Appendix A):

$$\eta = 0 : \quad S = 0, \quad \theta' = -1, \quad f' = -1, \quad (18a)$$

$$\eta \rightarrow \infty : \quad S' = 0, \quad \theta = 0, \quad f = 0, \quad (18b)$$

where the non-dimensional variables are

$$N_r = \frac{(\rho_p - \rho_{f\infty})kq_{np}}{(1 - \phi_{\infty})D_B\rho_{f\infty}\beta q_w}, \quad (19a)$$

$$N_b = \frac{\varepsilon(\rho c)_p q_{np}x}{(\rho c)_f \alpha_m Ra_x^{\frac{1}{3}}}, \quad (19b)$$

$$N_t = \frac{\varepsilon(\rho c)_p D_T q_w x}{(\rho c)_f k \alpha_m T_{\infty} Ra_x^{\frac{1}{3}}}, \quad (19c)$$

$$Le = \frac{\alpha_m}{\varepsilon D_B}. \quad (19d)$$

Because of the parameters N_b and N_t and the coordinate x along the plate, Eqs. (15)–(17) are locally similar. However, in the case of $\lambda = -0.5$ (i.e., both of the fluxes are proportional to $x^{-0.5}$), a true similarity solution is realized. This case (i.e., $\lambda = -0.5$) is selected to study the effects of the nanofluid parameters (i.e., Le , N_r , N_b , and N_t) on the velocity, the temperature, and the nanoparticle volume fraction of the boundary layer. In the case of $\lambda = -0.5$, Eqs. (15)–(17) are rewritten as follows:

$$S'' - \theta' + N_r f' = 0, \quad (20)$$

$$\theta'' + \frac{1}{2}S\theta' + N_b f' \theta' + N_t (\theta')^2 = 0, \quad (21)$$

$$f'' + \frac{1}{2}LeSf' + \frac{N_t}{N_b}\theta'' = 0. \quad (22)$$

It is notable that the system of Eqs. (20)–(22) is similar to the system obtained by Nield and Kuznetsov^[17]. Therefore, it is concluded that the governing equations in the case of heat and nanoparticle fluxes, both of which are proportional to $x^{-0.5}$, are similar to the governing equations in the case of constant surface temperature and constant surface nanoparticle concentration. However, the heat and concentration boundary conditions in the study of Nield and Kuznetsov^[17] are $\theta = 1$ and $f = 1$, while in the present study, they are $\theta' = -1$ and $f' = -1$. It is interesting that the integrating of Eq. (15) results in

$$S'(\eta) - \theta(\eta) + N_r f(\eta) = C, \quad (23a)$$

where C is a constant coming from the integration. From the boundary conditions in Eq. (18b), it can be obtained that the value of C is zero. Therefore, Eq. (23a) can be reduced to

$$S'(\eta) = \theta(\eta) - N_r f(\eta). \quad (23b)$$

Equation (23b) reveals that the velocity, the temperature, and the nanoparticle concentration in the boundary layer are directly connected to each other.

The quantities of the local Nusselt number (Nu_x) and the local Sherwood number (Sh_x), interested in the thermal engineering design of industrial equipments, can be defined as follows^[17]:

$$Nu_x = \frac{q_w x}{k(T_w - T_{\infty})}, \quad (24)$$

$$Sh_x = \frac{q_{np} x}{D_B(\phi_w - \phi_{\infty})}, \quad (25)$$

where q_w and q_{np} are the wall heat flux and the nanoparticle flux, respectively. With the similarity transforms introduced in Eq. (14), the reduced Nusselt number (Nu_r) and the reduced Sherwood number (Sh_r) are obtained as follows:

$$Nu_r = \frac{Nu_x}{Ra_x^{\frac{1}{3}}} = \frac{1}{\theta(0)}, \quad (26)$$

$$Sh_r = \frac{Sh_x}{Ra_x^{\frac{1}{3}}} = \frac{1}{f(0)}. \quad (27)$$

3 Results and discussion

The system of Eqs. (20)–(22) subjected to the boundary conditions (i.e., (18a) and (18b)) is considered and numerically solved for various ranges of N_r , N_b , and N_t and different values of Le . The numerical results are obtained by the finite difference method based on collocation points and Newton's method^[20–21].

Highly accurate solutions, with a relative tolerance of 10^{-6} , are achieved by an adaptive mesh scheme. An important criterion for the success of this numerical approach is to choose an appropriate finite value of η_∞ . Therefore, to estimate the realistic value of η_∞ , the solution process begins with an initial value of $\eta_\infty=4$, and Eqs. (20)–(22) are solved associated to the boundary conditions (18a) and (18b). The solution process is repeated to update the value of η_∞ until further changes (increment) in η_∞ cannot lead to any change in the values of the results or in other words, the results are independent of the value of the η_∞ . The results demonstrate that the choice of $\eta_{\max}=10$ guarantees that all numerical solutions approach to their asymptotic values.

Figure 2 shows the effects of variations of η_∞ on the reduced Nusselt number for selected values of non-dimensional parameters. In this figure, the values of η_∞ are chosen to be in the range of $4 < \eta_\infty < 10$, which is in accordance with the standard practice in the boundary layer analysis. Figure 2 depicts that as the finite value of η_∞ increases, the reduced Nusselt number tends to become a fixed value. Moreover, the effects of variations of η_∞ on the reduced Sherwood number are studied. It is found that the convergence trend is similar to the convergence trend of the reduced Nusselt number.

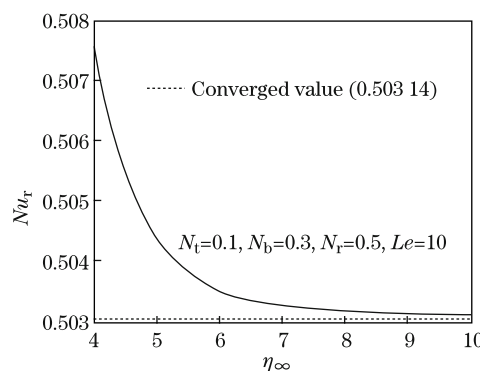


Fig. 2 Convergence trend of numerical method (reduced Nusselt number)

In the case of a constant surface heat flux (i.e., $\lambda=0$), when the effects of the thermophoresis, the Brownian motion, and the buoyancy ratio parameters are neglected, the model of the present study simulates the pure fluid which has been analyzed by Hassanien^[5] and Hsieh et al.^[6]. Therefore, as a test of the accuracy of the present solution, the values of Nu_r are compared

with those reported by Hassanien^[5] and Hsieh et al.^[6]. As listed in Table 1, the results are found to be in good agreement.

Table 1 Results for reduced Nusselt number $1/\theta(0)$

Hassanien ^[5]	Hsieh et al. ^[6]	Present results with $N_b=N_t=N_r=0$
0.771 579	0.771 5	0.771 545

In the case of a constant heat flux (i.e., $\lambda=0$), a comparison between the results of the present study when the nanofluid parameters are neglected (i.e., $N_r=N_b=N_t=0$) and the results reported by Hassanien^[5] is performed in Fig. 3. The zero values of m , n , and ξ in the work of Hassanien^[5] simulate a flat plate with a constant surface heat flux which is embedded in a saturated porous medium. Figure 3 depicts that the present results are in excellent agreement with the results presented by Hassanien^[5].

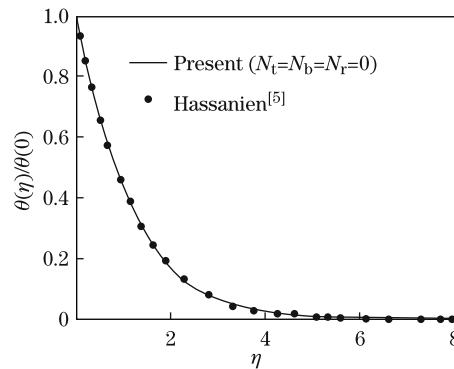


Fig. 3 Profiles of $\theta(\eta)/\theta(0)$ when nanofluid parameters are neglected

Since the thermal diffusivity of most nanofluids is much higher than the Brownian diffusion coefficient, the values of the Lewis number are comparatively high ($Le > 1$ ^[17]), the values of $Le=10$ and $Le=50$ are examined in the present study. The choice of values for N_r , N_b , and N_t is based on those values utilized by Nield and Kuznetsov^[17] for the case with the isothermal wall boundary condition. With the same values of N_r , N_b , and N_t , the present work with the heat flux boundary condition is viewed in proper perspective with the results for an isothermal plate.

The values of the reduced Nusselt number $1/\theta(0)$ and the reduced Sherwood number $1/f(0)$ are shown in Tables 2 and 3, respectively, for selected combinations of N_t , N_b , and N_r and for $Le=10$ and $Le=50$. The results in Table 2 indicate that the increase in the Brownian motion parameter, the thermophoresis parameter, or the buoyancy ratio parameter decreases the reduced Nusselt number. This table shows that an increase in the Lewis number increases the reduced Nusselt number. The variations of the reduced Nusselt number in Table 2 reveals that the effects of the Brownian motion and the thermophoresis parameters on the reduced Nusselt number are more than that of the buoyancy ratio parameter.

The results in Table 3 show that the reduced Sherwood number increases with the increase in N_b but decreases with the increase in N_r . This table depicts that for small values of N_b (i.e., $N_b=0.1$), the reduced Sherwood number first decreases, and then increases with the increase in the thermophoresis parameter. However, in the other combinations of N_r , N_b , and Le , an increase in the thermophoresis parameter increases the reduced Sherwood number. In addition, the increase in the Lewis number increases the reduced Sherwood number. It is worth

mentioning that the increase in the Lewis number has a significant effect on the reduced Sherwood number in comparison with its effect on the reduced Nusselt number. Furthermore, Nield and Kuznetsov^[17] found that the increases in N_t , N_b , and N_r decreased the reduced Nusselt number.

Table 2 Effects of N_b , N_t , N_r , and Le on reduced Nusselt number

N_b	N_t	$N_r=0.1$		$N_r=0.3$		$N_r=0.5$	
		$Le=10$	$Le=50$	$Le=10$	$Le=50$	$Le=10$	$Le=50$
0.1	0.1	0.535 23	0.545 14	0.528 09	0.543 64	0.520 72	0.542 11
	0.2	0.504 76	0.515 36	0.495 68	0.513 45	0.486 39	0.511 53
	0.3	0.474 74	0.485 19	0.464 51	0.483 04	0.454 08	0.480 87
	0.4	0.445 05	0.454 54	0.434 33	0.452 30	0.423 46	0.450 04
	0.5	0.415 55	0.423 36	0.404 93	0.421 15	0.394 18	0.418 93
0.3	0.1	0.512 56	0.532 80	0.507 92	0.531 73	0.503 14	0.530 65
	0.2	0.484 06	0.503 65	0.479 16	0.502 52	0.474 16	0.501 38
	0.3	0.455 68	0.474 04	0.450 73	0.472 90	0.445 73	0.471 74
	0.4	0.427 32	0.443 89	0.422 51	0.442 78	0.417 67	0.441 66
	0.5	0.398 88	0.413 15	0.394 36	0.412 10	0.389 84	0.411 06
0.5	0.1	0.490 87	0.520 82	0.486 88	0.519 83	0.482 79	0.518 83
	0.2	0.463 56	0.492 14	0.459 62	0.491 16	0.455 61	0.490 17
	0.3	0.436 25	0.462 97	0.432 46	0.462 03	0.428 63	0.461 07
	0.4	0.408 85	0.433 25	0.405 31	0.432 36	0.401 74	0.431 46
	0.5	0.381 30	0.402 91	0.378 07	0.402 10	0.374 84	0.401 29

Table 3 Effects of N_b , N_t , N_r , and Le on reduced Sherwood number

N_b	N_t	$N_r=0.1$		$N_r=0.3$		$N_r=0.5$	
		$Le=10$	$Le=50$	$Le=10$	$Le=50$	$Le=10$	$Le=50$
0.1	0.1	1.806 93	4.665 83	1.779 37	4.636 47	1.750 72	4.606 52
	0.2	1.607 48	4.478 97	1.584 68	4.455 08	1.561 29	4.430 80
	0.3	1.520 67	4.494 59	1.501 90	4.475 94	1.482 81	4.457 09
	0.4	1.514 19	4.711 53	1.498 62	4.697 90	1.482 62	4.684 18
	0.5	1.584 04	5.183 71	1.570 06	5.174 36	1.554 96	5.164 94
0.3	0.1	2.178 95	5.141 30	2.152 13	5.110 97	2.124 40	5.080 10
	0.2	2.141 14	5.194 13	2.118 94	5.167 76	2.096 19	5.140 97
	0.3	2.153 79	5.340 56	2.136 05	5.318 13	2.118 03	5.295 41
	0.4	2.218 15	5.594 77	2.204 70	5.576 28	2.191 16	5.557 59
	0.5	2.342 91	5.983 93	2.333 48	5.969 27	2.324 06	5.954 51
0.5	0.1	2.314 33	5.297 35	2.288 94	5.267 61	2.262 80	5.237 37
	0.2	2.333 50	5.415 54	2.312 13	5.389 17	2.290 27	5.362 41
	0.3	2.389 17	5.601 83	2.371 75	5.578 83	2.354 05	5.555 55
	0.4	2.486 40	5.869 00	2.472 84	5.849 36	2.459 17	5.829 51
	0.5	2.634 72	6.236 85	2.624 90	6.220 49	2.615 06	6.204 00

It is well-known that for a conventional pure fluid, the boundary-layer profiles of θ and the profiles of $ds/d\eta$ (something that represents the longitudinal component of the velocity u) are identical^[2,17]. The dimensionless profiles for a pure fluid and a nanofluid are compared in Fig. 4 when $N_t=N_b=N_r=0.5$ and $Le=10$. This figure shows that the thickness of the boundary layer

for the concentration profile is much smaller than the thickness of the non-dimensional thermal and velocity boundary layers. Furthermore, the profiles of the dimensionless temperature and velocity are not identical in the case of nanofluids. These findings are in good agreement with the results of the case of an isothermal plate reported by Nield and Kuznetsov^[17].

The two-dimensional streamline profiles for a pure fluid and a nanofluid are plotted in Fig. 5. As seen from the figure, the streamline profiles near the plate are close together, which shows that the velocity near the plate is high. The streamline profiles near the plate are comparatively parallel to the plate, which confirms the impermeability condition of the plate surface. The streamline profiles of the pure fluid and the nanofluid have a comparatively same pattern. However, they are not identical.

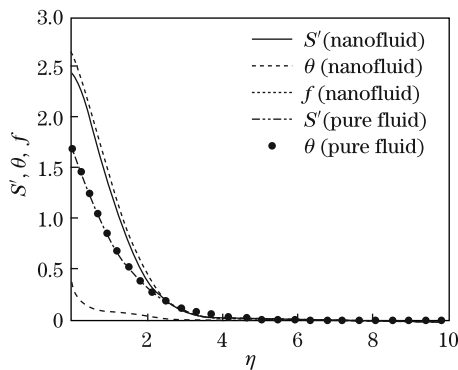


Fig. 4 Boundary layer profiles of nanofluid ($N_t=N_b=N_r=0.5$ and $Le=10$) and pure fluid

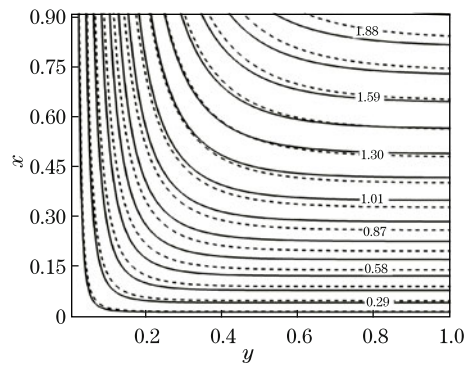


Fig. 5 Streamline profiles of nanofluid ($N_t=0.1$, $N_b=0.3$, $N_r=0.5$, $Le=10$, and $\lambda=-0.5$) and pure fluid ($\lambda=-0.5$) where solid lines are for nanofluid and dashed lines are for pure fluid

The thermophoresis parameter N_t can be described as the ratio of the nanoparticle diffusion, which is due to the thermophoresis effect, to the thermal diffusion in the nanofluid. According to Buongiorno's report^[22], the solid particles in the fluid experience a force in the direction opposite to the imposed temperature gradient. Therefore, the particles tend to move from hot to cold. The increase in the nanoparticle concentration by the increase in the thermophoresis effect results in the increase in the temperature profiles and consequently the increase in the velocity profiles. The thermophoresis parameter is independent of the particle diameter in the case of very small particles. The profiles of the concentration, the dimensionless velocity, and the temperature for different values of N_t are plotted in Figs. 6, 7, and 8, respectively, when $N_b=0.3$, $N_r=0.5$, and $Le=10$. These figures reveal that the increase in N_t increases the magnitude of the dimensionless temperature, the velocity, and the magnitude of the concentration profiles. This is because of the fact that the thermophoresis force, which tends to move particles from the hot zone to the cold zone, increases with the increase in N_t , which results in that the increase in the thermophoresis force increases the nanoparticle concentration, as seen in Fig. 6. Furthermore, the increase in the nanoparticle diffusion into the fluid increases the magnitude of the dimensionless temperature, as shown in Fig. 8.

The Brownian motion parameter can be described as the ratio of the nanoparticle diffusion, which is due to the Brownian motion effect, to the thermal diffusion in the nanofluid. Therefore, it is expected that the Brownian motion parameter increases with an increase in the difference between the nanoparticle volume fractions at the wall and ambient. Based on the Einstein-Stokes equation^[22], the Brownian motion is proportional to the inverse of the particle diameter^[22]. Hence, as the particle diameter decreases, the Brownian motion increases. The

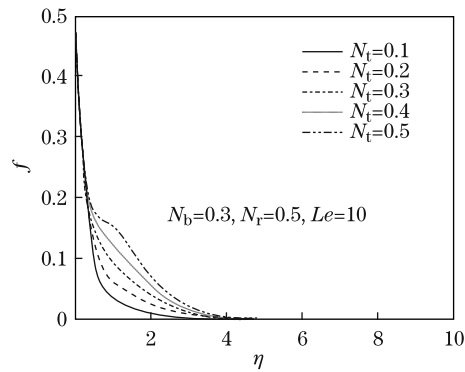


Fig. 6 Concentration profiles for various N_t

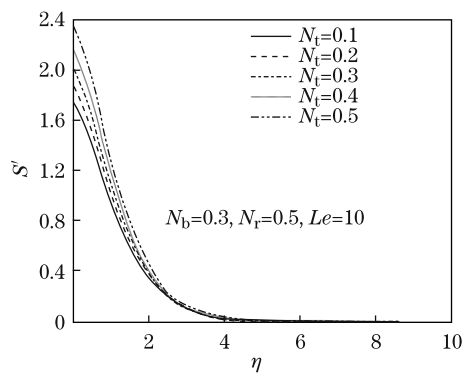


Fig. 7 Velocity profiles for various N_t

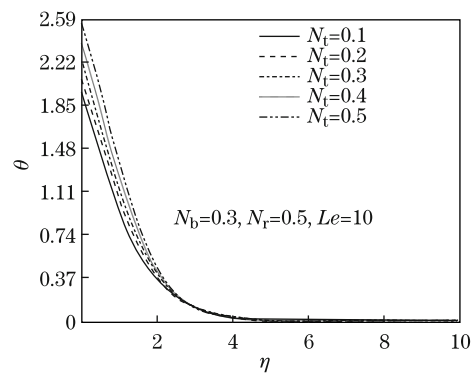


Fig. 8 Temperature profiles for various N_t

profiles of the concentration, the dimensionless velocity, and the temperature for different values of the Brownian motion parameter are depicted in Figs. 9, 10, and 11, respectively, when $N_t = 0.1$, $N_r = 0.5$, and $Le = 10$. These figures reveal that the increase in N_b increases the dimensionless velocity and temperature profiles whereas decreases the nanoparticle concentration profiles. Comparisons between Figs. 9, 10, and 11 show that the effects of variations of N_b on the variations of concentration profiles are much higher than those effects on the dimensionless velocity and temperature profiles. Generally, the increase in N_b tends to decrease the nanoparticle concentration, as shown in Fig. 9. The diffusion of nanoparticles into the fluid increases with the increase in N_b , and thereby, the velocity and temperature profiles are increased, as shown in Figs. 10 and 11, respectively.

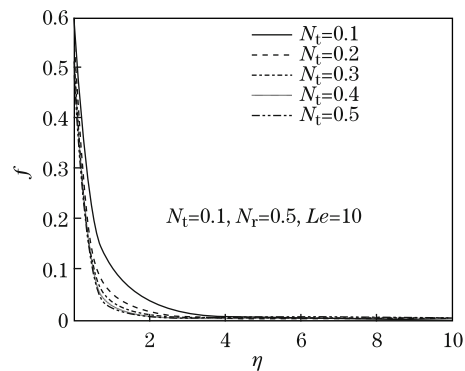
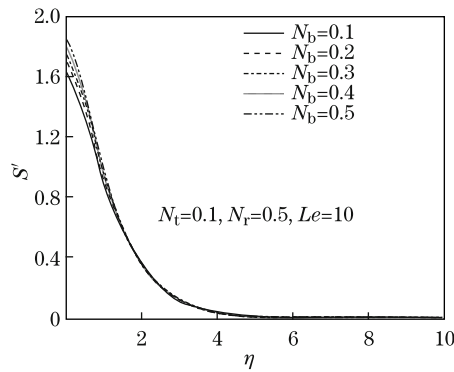
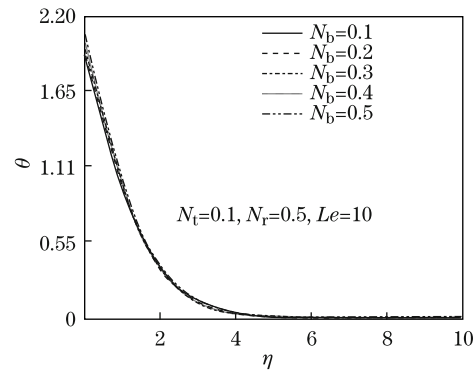
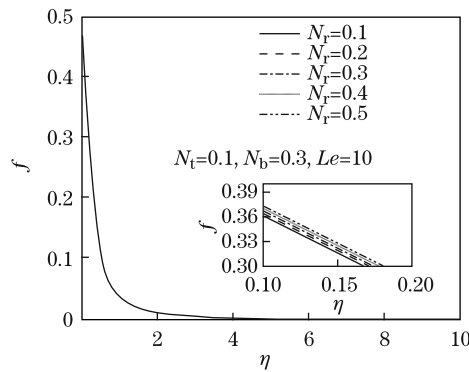
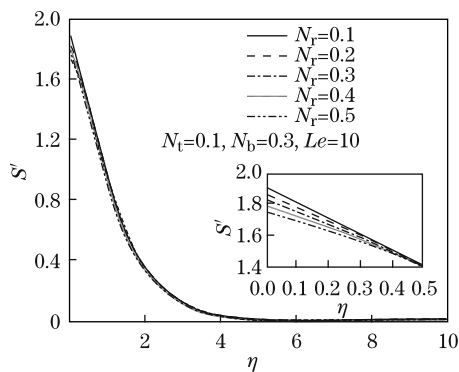
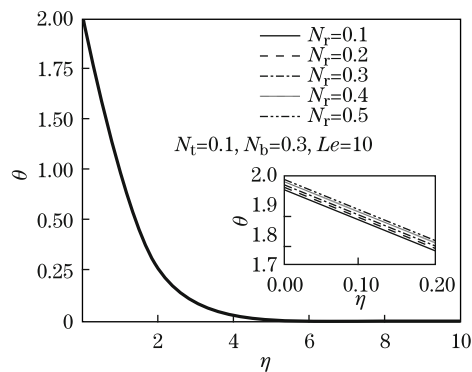


Fig. 9 Concentration profiles for various N_b

**Fig. 10** Velocity profiles for various N_b **Fig. 11** Temperature profiles for various N_b

The buoyancy-ratio parameter can be described as the ratio of the variation of the fluid density, which is due to the variation of the concentration, to the variation of the density of the nanofluid, which is due to the variation of temperature. The profiles of the concentration, the dimensionless velocity, and the temperature for different values of the buoyancy-ratio parameter are plotted in Figs. 12–14, respectively, when $N_b=0.3$, $N_t=0.1$, and $Le=10$. These figures show that an increase in the Buoyancy-ratio parameter increases the magnitude of the dimensionless concentration and temperature profiles while decreases the magnitude of the dimensionless velocity profiles. The increase in the velocity profiles is in good agreement with Eq. (23b). From Figs. 12–14, it is clear that the variations of the buoyancy-ratio parameter have small effects on the dimensionless velocity, the temperature, and the concentration.

**Fig. 12** Concentration profiles for various N_r **Fig. 13** Velocity profiles for various N_r **Fig. 14** Temperature profiles for various N_r

It is worth mentioning that the consideration of additional heat transfer mechanisms in the convective heat transfer problems has been further developed by Buongiorno^[22]. Buongiorno^[22] discussed seven possible mechanisms which affect the convection of nanofluids because of the movement of nanoparticles in the base fluid. Of all the mechanisms, the thermophoresis and the Brownian diffusion are found to be important^[23]. As seen in Figs. 6–14 and Table 2, the variations of the thermophoresis parameter N_t and the Brownian motion parameter N_b impress the variations of the dimensionless velocity, the temperature, and the concentration. The same results are observed for the reduced Nusselt number and the reduced Sherwood number. These findings are in good agreement with Buongiorno's report^[22].

Comparisons between the three boundary layers shown in Figs. 6–14 demonstrate that the thermal and velocity boundary layers are of comparable thickness. However, they are not identical. The nanoparticle concentration boundary layer is much thinner than the thermal and velocity boundary layers.

Figure 15 depicts the effect of N_b on the reduced Nusselt number in the cases of $Le=10$ and $Le=50$, respectively, for a variation of the thermophoresis parameter N_t . The figure reveals that the increase in the thermophoresis parameter decreases the reduced Nusselt number. In both cases of $Le=10$ and $Le=50$, the increase in the Brownian motion parameter decreases the reduced Nusselt number. The variation of the reduced Nusselt number with N_b and N_t is due to the effects of N_b and N_t on the magnitude of the dimensionless temperature on the wall, as shown in Figs. 8 and 11. According to Eq. (26), with the increase in N_b or N_t , the dimensionless temperature increases, and thereby, the reduced Nusselt number decreases. Furthermore, the increase in the Lewis number increases the reduced Nusselt number.

The effects of N_b , N_t , and Le on the reduced Sherwood number are depicted in Fig. 16. According to this figure, the increase in the thermophoresis parameter decreases the reduced Sherwood number. The increase in the Lewis number increases the reduced Sherwood number for selected values of N_t and N_b , which are shown in Fig. 16. This figure demonstrates that the reduced Sherwood number increases with the increase in N_b . This increase confirms the results of Fig. 9, which shows that the increase in N_b decreases the magnitude of the nanoparticle concentration. Therefore, according to Eq. (27), the reduced Sherwood number increases with the increase in N_b .

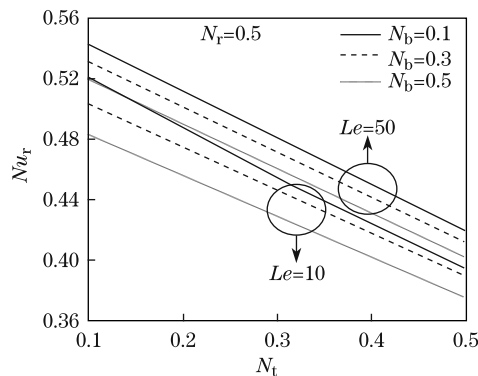


Fig. 15 Effects of N_b and Le on dimensionless heat transfer rate

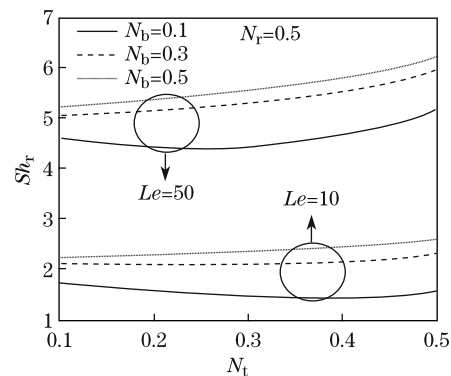


Fig. 16 Effects of N_b and Le on reduced Sherwood number

4 Conclusions

In this paper, the influence of nanoparticles on the natural convection boundary layer of a vertical flat plate embedded in a porous medium saturated by a nanofluid is investigated. In the

nanofluid model, the Brownian motion and thermophoresis forces are taken into account. In the case of a surface heat flux and a surface nanoparticle flux, the governing differential equations are reduced to a set of coupled ordinary differential equations by the similarity transforms. The conclusions can be summarized as follows:

(i) In contrast with the temperature and velocity profiles of the pure fluids, which are identical, the temperature and velocity profiles in the nanofluids are of comparable thickness. However, they are not identical, and the nanoparticle concentration boundary layer is much thinner than the pure fluid concentration boundary layer.

(ii) The reduced Nusselt number decreases with an increase in the Brownian motion parameter, the thermophoresis parameter, or the buoyancy ratio parameter, whereas it increases with an increase in the Lewis number.

(iii) In most cases, the reduced Sherwood number increases with an increase in the thermophoresis parameter. However, it first decreases, and then increases with the increase in the thermophoresis parameter when the Brownian motion parameters is comparatively small (i.e., $N_b=0.1$).

(iv) The reduced Sherwood number increases with an increase in N_b or Le , whereas decreases with an increase in N_r .

(v) The effect of the variation of the Brownian motion or the thermophoresis parameter on the variation of the reduced Nusselt number is more than that of the buoyancy ratio parameter.

Acknowledgements The authors are grateful to Shahid Chamran University of Ahvaz for its support of this paper.

References

- [1] Gorla, R. S. R., Chamkha, A. J., and Rashad, A. M. Mixed convective boundary layer flow over a vertical wedge embedded in a porous medium saturated with a nanofluid: natural convection dominated regime. *Nanoscale Research Letters*, **6**, 1–9 (2011)
- [2] Cheng, P. and Minkowycz, W. J. Free convection about a vertical flat plate embedded in a porous medium with application to heat transfer from a dike. *Journal of Geophysical Research*, **82**, 2040–2044 (1977)
- [3] Bejan, A. and Khair, K. R. Heat and mass transfer by natural convection in a porous medium. *International Journal of Heat and Mass Transfer*, **28**, 909–918 (1985)
- [4] Kaviani, M. and Mittal, M. An experimental study of vertical plate natural convection in porous media. *Heat Transfer in Porous Media and Particulate Flows*, **46**, 175–179 (1985)
- [5] Hassanien, I. A. Variable permeability effects on mixed convection along a vertical wedge embedded in a porous medium with variable surface heat flux. *Applied Mathematics and Computation*, **138**, 41–59 (2003)
- [6] Hsieh, C., Chen, T. S., and Armaly, B. F. Non similarity solutions for mixed convection from vertical surfaces in porous media: variable surface temperature or heat flux. *International Journal of Heat and Mass Transfer*, **36**, 1485–1493 (1993)
- [7] Lee, S., Choi, S. U. S., Li, S., and Eastman, J. A. Measuring thermal conductivity of fluids containing oxide nanoparticles. *Journal of Heat Transfer*, **121**, 280–289 (1999)
- [8] Wang, X., Xu, X., and Choi, S. U. S. Thermal conductivity of nanoparticle-fluid mixture. *Journal of Thermophysics and Heat Transfer*, **13**, 474–480 (1999)
- [9] Li, C. H. and Peterson, G. P. The effect of particle size on the effective thermal conductivity of Al_2O_3 -water nanofluids. *Journal of Applied Physics*, **101**, 1–5 (2007)
- [10] Saidur, R., Leong, K. Y., and Mohammad, H. A. A review on applications and challenges of nanofluids. *Renewable and Sustainable Energy Reviews*, **15**, 1646–1668 (2011)
- [11] Noghrehabadi, A., Behseresht, A., and Ghalambaz, M. Natural convection flow of nanofluids over a vertical cone embedded in a non-Darcy porous medium. *Journal of Thermophysics and Heat Transfer*, **27**, 334–341 (2013)

- [12] Noghrehabadi, A., Ghalambaz, M., and Ghanbarzadeh, A. Heat transfer of magnetohydrodynamic viscous nanofluids over an isothermal stretching sheet. *Journal of Thermophysics and Heat Transfer*, **26**, 686–689 (2012)
- [13] Noghrehabadi, A., Ghalambaz, M., Ghalambaz, M., and Ghanbarzadeh, A. Comparing thermal enhancement of Ag-water and SiO₂-water nanofluids over an isothermal stretching sheet with suction or injection. *Journal of Computational and Applied Research in Mechanical Engineering*, **2**, 35–47 (2012)
- [14] Noghrehabadi, A., Pourrajab, R., and Ghalambaz, M. Effect of partial slip boundary condition on the flow and heat transfer of nanofluids past stretching sheet prescribed constant wall temperature. *International Journal of Thermal Science*, **54**, 253–261 (2012)
- [15] Ahmad, S. and Pop, I. Mixed convection boundary layer flow from a vertical flat plate embedded in a porous medium filled with nanofluids. *International Communications in Heat and Mass Transfer*, **37**, 987–991 (2010)
- [16] Hady, F. M., Ibrahim, F. S., Abdel-Gaied, S. M., and Eid, M. R. Effect of heat generation/absorption on natural convective boundary-layer flow from a vertical cone embedded in a porous medium filled with a non-Newtonian nanofluid. *International Communications in Heat and Mass Transfer*, **30**, 1414–1420 (2011)
- [17] Nield, D. A. and Kuznetsov, A. V. The Cheng-Minkowycz problem for natural convective boundary-layer flow in a porous medium saturated by a nanofluid. *International Journal of Heat and Mass Transfer*, **52**, 5792–5795 (2009)
- [18] Gorla, R. S. R. and Chamkha, A. J. Natural convective boundary layer flow over a horizontal plate embedded in a porous medium saturated with a nanofluid. *Journal of Modern Physics*, **2**, 62–71 (2011)
- [19] Sivasamy, A., Selladuria, V., and Kanna, P. R. Mixed convection on jet impingement cooling of a constant heat flux horizontal porous layer. *International Journal of Thermal Science*, **49**, 1238–1246 (2010)
- [20] Keller, H. B. *Numerical Solution of Two-Point Boundary Value Problems*, University City Science Center, Philadelphia (1976)
- [21] Russell, R. D. and Shampine, L. F. A collocation method for boundary value problems. *Numerische Mathematik*, **19**, 1–28 (1972)
- [22] Buongiorno, J. Convective transport in nanofluids. *Journal of Heat Transfer*, **128**, 240–250 (2006)
- [23] Das, S. K., Choi, S. U. S., Yu, W., and Pradeep, T. *Nanofluids — Science and Technology*, John Wiley & Sons, New Jersey, 1–39 (2007)

Appendix A

By cross-differentiation and Eq. (8), the momentum equation (2) can be simplified as

$$\frac{\partial^2 \psi}{\partial y^2} = \frac{(1 - \phi_\infty) \rho_{f\infty} \beta g K}{\mu} \frac{\partial T}{\partial y} - \frac{(\rho_p - \rho_{f\infty}) g K}{\mu} \frac{\partial \phi}{\partial y}. \quad (\text{A1})$$

By substituting the introduced similarity variables in Eqs. (13) and (14), each term of Eq. (A1) can be written as follows:

$$\frac{\partial \eta}{\partial y} = \frac{Ra_x^{\frac{1}{3}}}{x}, \quad (\text{A2})$$

$$\frac{\partial \psi}{\partial S} = \alpha_m Ra_x^{\frac{1}{3}}, \quad (\text{A3})$$

$$\frac{\partial \psi}{\partial y} = \frac{\partial \psi}{\partial S} \frac{\partial S}{\partial \eta} \frac{\partial \eta}{\partial y} = \left(\alpha_m Ra_x^{\frac{1}{3}} \right) \left(\frac{Ra_x^{\frac{1}{3}}}{x} \right) S' = \alpha_m \frac{Ra_x^{\frac{2}{3}}}{x} S', \quad (\text{A4})$$

$$\frac{\partial^2 \psi}{\partial y^2} = \frac{\partial}{\partial y} \left(\frac{\partial \psi}{\partial y} \right) = \left(\alpha_m \frac{Ra_x^{\frac{2}{3}}}{x} \right) \frac{\partial S'}{\partial \eta} \frac{\partial \eta}{\partial y} = \alpha_m \frac{Ra_x}{x^2} S'', \quad (\text{A5})$$

$$\frac{\partial T}{\partial y} = \frac{\partial T}{\partial \theta} \frac{\partial \theta}{\partial \eta} \frac{\partial \eta}{\partial y} = \left(\frac{q_w x}{k_m} Ra_x^{-\frac{1}{3}} \right) \left(\frac{Ra_x^{\frac{1}{3}}}{x} \right) \theta' = \frac{q_w}{k_m} \theta', \quad (A6)$$

$$\frac{\partial \phi}{\partial y} = \frac{\partial \phi}{\partial f} \frac{\partial f}{\partial \eta} \frac{\partial \eta}{\partial y} = \left(\frac{q_{np} x}{D_B} \right) Ra_x^{-\frac{1}{3}} \left(\frac{Ra_x^{\frac{1}{3}}}{x} \right) f' = \frac{q_{np}}{D_B} f'. \quad (A7)$$

By substituting Eqs. (A5)–(A7) into Eq. (A1), the following equation can be obtained:

$$\alpha_m \frac{Ra_x}{x^2} S'' = \frac{(1 - \phi_\infty) \rho_{f\infty} \beta g K}{\mu} \frac{q_w}{k} \theta' - \frac{(\rho_p - \rho_{f\infty}) g K}{\mu} \frac{q_{np}}{D_B} f'. \quad (A8)$$

Divided by $\alpha_m \frac{Ra}{x^2}$, Eq. (A8) can be simplified as follows:

$$S'' = \theta' - \frac{(\rho_p - \rho_{f\infty}) k q_{np}}{(1 - \phi_\infty) D_B \rho_{f\infty} \beta q_w} f', \quad (A9)$$

$$S'' - \theta' + N_r f' = 0, \quad (A10)$$

where

$$N_r = \frac{(\rho_p - \rho_{f\infty}) k q_{np}}{(1 - \phi_\infty) \rho_{f\infty} \beta D_B q_w}. \quad (A11)$$

By use of the similarity variables of Eqs. (13) and (14), each term of Eq. (3) can be evaluated as follows:

$$\frac{\partial \eta}{\partial x} = \frac{\lambda - 1}{3} \frac{y}{x^2} Ra_x^{\frac{1}{3}}, \quad (A12)$$

$$\begin{aligned} \frac{\partial T}{\partial x} &= (\lambda + 1) \frac{q_w}{k_m} Ra_x^{-\frac{1}{3}} \theta + \frac{q_w x}{k_m} \theta \frac{\partial}{\partial x} \left(Ra_x^{-\frac{1}{3}} \right) + \frac{q_w x}{k_m} Ra_x^{-\frac{1}{3}} \frac{\partial \theta}{\partial \eta} \frac{\partial \eta}{\partial x} \\ &= (\lambda + 1) \frac{q_w}{k_m} Ra_x^{-\frac{1}{3}} \theta - \frac{\lambda + 2}{3} \frac{q_w Ra_x^{-\frac{1}{3}}}{k_m} \theta + \frac{q_w (\lambda - 1) y}{3 k x} \theta', \end{aligned} \quad (A13)$$

$$\begin{aligned} \frac{\partial \psi}{\partial x} &= S \frac{\partial}{\partial x} \left(\alpha_m Ra_x^{\frac{1}{3}} \right) + \alpha_m Ra_x^{\frac{1}{3}} \frac{\partial S}{\partial \eta} \frac{\partial \eta}{\partial x} \\ &= \frac{\lambda - 1}{3} \alpha_m y \frac{Ra_x^{\frac{2}{3}}}{x^2} S' + \frac{\lambda + 2}{3} \alpha_m \frac{Ra_x^{\frac{1}{3}}}{x} S, \end{aligned} \quad (A14)$$

$$\begin{aligned} \frac{\partial^2 T}{\partial y^2} &= \frac{\partial}{\partial y} \left(\frac{\partial T}{\partial y} \right) \\ &= \frac{q_w}{k} \frac{\partial \theta'}{\partial \eta} \frac{\partial \eta}{\partial y} \\ &= \frac{q_w Ra_x^{\frac{1}{3}}}{k x} \theta'', \end{aligned} \quad (A15)$$

$$\left(\frac{\partial T}{\partial y} \right)^2 = \frac{q_w^2}{k_m^2} \theta'^2. \quad (A16)$$

By substituting Eqs. (A4), (A6), (A7), and (A13)–(A16) in Eq. (12), the following equation can be

obtained:

$$\begin{aligned}
 & \alpha_m \frac{Ra_x^{\frac{2}{3}}}{x} S' \left((\lambda + 1) \frac{q_w}{k_m} Ra_x^{-\frac{1}{3}} \theta - \frac{\lambda + 2}{3k_m} q_w Ra_x^{-\frac{1}{3}} \theta \right. \\
 & \quad \left. + \frac{q_w}{k} \frac{\lambda - 1}{3} \frac{y}{x} \theta' \right) \\
 & \quad - \left(\frac{\lambda - 1}{3} \alpha_m y \frac{Ra_x^{\frac{2}{3}}}{x^2} S' + \frac{\lambda + 2}{3} \alpha_m \frac{Ra_x^{\frac{1}{3}}}{x} S \right) \frac{q_w}{k_m} \theta' \\
 & = \alpha_m \frac{q_w}{k_m} \frac{Ra_x^{\frac{1}{3}}}{x} \theta'' + \tau q_{np} S' \frac{q_w}{k_m} \theta' + \tau \frac{D_T}{T_\infty} \left(\frac{q_w}{k_m} \theta' \right)^2.
 \end{aligned} \tag{A17}$$

With simple manipulation and division by $\alpha_m \frac{q_w}{k_m} \frac{Ra_x^{\frac{1}{3}}}{x}$, Eq. (A17) can be simplified as follows:

$$\begin{aligned}
 & \frac{2\lambda + 1}{3} S' \theta - \frac{\lambda + 2}{3} S \theta' \\
 & = \theta'' + \tau \left(q_{np} S' \frac{x}{\alpha_m Ra_x^{\frac{1}{3}}} \theta' + \frac{D_T}{T_\infty} \frac{q_w}{k_m} \frac{x}{\alpha_m Ra_x^{\frac{1}{3}}} \theta'^2 \right),
 \end{aligned} \tag{A18}$$

$$\theta'' + \frac{\lambda + 2}{3} S \theta' - \frac{2\lambda + 1}{3} S' \theta + N_b f' \theta' + N_t \theta'^2 = 0, \tag{A19}$$

where

$$\begin{cases} N_b = \frac{\varepsilon (\rho c)_p q_{np} x}{(\rho c)_f \alpha_m Ra_x^{\frac{1}{3}}}, \\ N_t = \frac{\varepsilon (\rho c)_p D_T q_w x}{(\rho c)_f \alpha_m T_\infty k_m Ra_x^{\frac{1}{3}}}. \end{cases} \tag{A20}$$

Two terms of conservation of the nanoparticle equation (4) can be evaluated as follows:

$$\begin{aligned}
 \frac{\partial^2 \phi}{\partial y^2} & = \frac{\partial}{\partial y} \left(\frac{q_{np}}{D_B} f' \right) \\
 & = \frac{q_{np}}{D_B} \frac{\partial f'}{\partial \eta} \frac{\partial \eta}{\partial y} \\
 & = \frac{q_{np}}{D_B} \frac{Ra_x^{\frac{1}{3}}}{x} f'',
 \end{aligned} \tag{A21}$$

$$\begin{aligned}
 \frac{\partial \phi}{\partial x} & = \frac{q_{np} x}{D_B} Ra_x^{-\frac{1}{3}} \frac{\partial f}{\partial \eta} \frac{\partial \eta}{\partial x} + (\lambda + 1) \frac{q_{np}}{D_B} Ra_x^{-\frac{1}{3}} f + \frac{q_{np} x}{D_B} f \frac{\partial}{\partial x} \left(Ra_x^{-\frac{1}{3}} \right) \\
 & = \frac{q_{np}}{D_B} \frac{\lambda - 1}{3} \frac{y}{x} f' + (\lambda + 1) \frac{q_{np}}{D_B} Ra_x^{-\frac{1}{3}} f - \frac{\lambda + 2}{3} \frac{q_{np}}{D_B} Ra_x^{-\frac{1}{3}} f.
 \end{aligned} \tag{A22}$$

By substituting Eqs. (A4), (A7), (A14), (A15), (A21), and (A22) in Eq. (4), the following equation

can be obtained:

$$\begin{aligned}
 & \alpha_m \frac{Ra_x^{\frac{2}{3}}}{x} S' \left(\frac{q_{np}}{D_B} \frac{\lambda-1}{3} \frac{y}{x} f' \right. \\
 & \quad \left. + (\lambda+1) \frac{q_{np}}{D_B} Ra_x^{-\frac{1}{3}} f - \frac{\lambda+2}{3} \frac{q_{np}}{D_B} Ra_x^{-\frac{1}{3}} f \right) \\
 & \quad - \left(\frac{\lambda-1}{3} \alpha_m y \frac{Ra_x^{\frac{2}{3}}}{x^2} S' + \frac{\lambda+2}{3} \alpha_m \frac{Ra_x^{\frac{1}{3}}}{x} S \right) \frac{q_{np}}{D_B} f' \\
 & = q_{np} \frac{Ra_x^{\frac{1}{3}}}{x} f'' + \frac{D_T}{T_\infty} \frac{q_w}{k_m} \frac{Ra_x^{\frac{1}{3}}}{x} \theta''.
 \end{aligned} \tag{A23}$$

Divided by $\frac{Ra_x^{\frac{1}{3}} q_{np}}{x}$, Eq. (A23) can be simplified as follows:

$$-\frac{\lambda+2}{3} \frac{\alpha_m}{\varepsilon D_B} S f' + \frac{2\lambda+1}{3} \frac{\alpha_m}{\varepsilon D_B} f S' = f'' + \frac{D_T q_w x}{T_\infty k_m q_{np} x} \theta'', \tag{A24}$$

$$f'' + \frac{\lambda+2}{3} Le S f' - \frac{2\lambda+1}{3} Le f S' + \frac{N_t}{N_b} \theta'' = 0, \tag{A25}$$

where

$$\begin{cases} \frac{N_t}{N_b} = \frac{D_T q_w x}{T_\infty k_m q_{np} x}, \\ Le = \frac{\alpha_m}{\varepsilon D_B}. \end{cases} \tag{A26}$$